Performance Analysis of Multi-Band Microwave and Millimeter-Wave Operation in 5G NR Systems

V. Begishev, E. Sopin, D. Moltchanov, R. Pirmagomedov, A. Samuylov, S. Andreev, Y. Koucheryavy, and K. Samouylov

***Abstract*—Blockage of millimeter-wave (mmWave) radio propagation paths in dense mobile scenarios requires advanced techniques to preserve session continuity in 5G New Radio (NR) systems. In this work, we employ the tools of stochastic geometry and queuing theory as well as rely on 3GPP cluster-based propagation modeling to formulate a mathematical framework, which captures session-level service dynamics of user equipment (UE) that supports multi-band operation. Accordingly, the sub-6 GHz NR base station (BS) is used to temporarily serve the sessions with strict throughput requirements that experience an outage at the mmWave NR BSs. We derive user- and system-centric key performance indicators, including new and ongoing session drop probabilities as well as radio resource utilization. Our numerical results confirm that the use of microwave BSs to serve mmWave sessions is only feasible in light traffic conditions. Particularly, the presence of throughput-hungry mmWave traffic increases the session drop probability at the sub-6 GHz band as well as decreases its utilization. Further, the support of sub-6 GHz radio may not improve the mmWave BS resource utilization, as many mmWave sessions are dropped during their service as a consequence of frequent blockage-induced outage situations.**

I. Introduction

The sub-6 GHz 5G New Radio (NR) systems are currently being deployed across the world, thus initiating the first phase of 5G market penetration [1], [2]. However, to fully satisfy the ITU performance requirements [3], the available spectrum below 6 GHz may be insufficient [4]. Following the NR implementation guidelines specified in [5] by the GSMA consortium, the utilization of millimeter-wave (mmWave) bands is essential to provide the required capacity. However, mmWave-based transmissions are susceptible to higher propagation losses. The latter, combined with higher sensitivity to link blockages, may reduce coverage of a mmWave NR base station (BS). This problem becomes more pronounced in *dynamic* blockage environments, such as crowded streets or urban squares.

V. Begishev, E. Sopin, A. Samuylov, and K. Samouylov are with Peoples' Friendship University of Russia (RUDN University), 6 Miklukho-Maklaya St, Moscow, 117198, Russian Federation. Email: {begishev-vo, sopin-es, samuylov-ak, samuylov-ke}@rudn.ru. K. Samouylov and E. Sopin are also with Federal Research Center "Computer Science and Control" of the Russian Academy of Sciences (FRC CSC RAS), 44-2 Vavilov St, Moscow, 119333, Russian Federation. D. Moltchanov, R. Pirmagomedov, S. Andreev, and Y. Koucheryavy are with Tampere University, Finland. Email: {firstname.lastname}@tuni.fi. Y. Koucheryavy is also with Higher School of Economics, Moscow, Russian Federation.

The publication was supported by the Russian Science Foundation (agreement No 18-19-00580, Section III, V, VI). This work was supported by 5G-Force Business Finland project. This work was supported by the Academy of Finland (Project RADIANT). This paper has been supported by the RUDN University Strategic Academic Leadership Program (recipient K.Samouylov, supervision, project administration). The reported study was funded by RFBR, project number 20-07-01052 (recipient E.Sopin, mathematical model development) and project number 20-07-01064 (recipient V.Begishev, visualisation).

Recent empirical [6] and theoretical [7] studies have deeply investigated the effects of link blockage in various mmWave deployments. Notably, it has been demonstrated that the signal-to-noise ratio (SNR) level may rapidly fluctuate by 10-30 dB at sub-second time scales, which can cause frequent service outages [8]. Such outage events interrupt the ongoing session service, which drastically harms the overall user experience [9].

3GPP envisions two approaches for alleviating the impact of outages. The first, intra-RAT approach relies on the multi-connectivity functionality ratified as part of 5G system design [10]. According to the specifications, user equipment (UE) can maintain multiple simultaneous connections with the nearest BSs. When the currently active link experiences outage conditions, the packet flow can be rerouted to a backup connection. For standalone mmWave-based NR systems, the utilization of this functionality requires a dense deployment of BSs and thus may not be suitable for early 5G NR rollouts. Furthermore, it has recently been shown that the respective session continuity might be compromised even in dense deployments [11].

As an alternative approach, vendors consider the support of multiple concurrent RATs at the UE via multi-band operation enabled by the standardized carrier aggregation functionality [12]. Such multi-band access has been demonstrated recently in both 3.5 and 28 GHz 5G NR bands[1]. The presented solution alleviates the impact of outages by instantly rerouting the traffic to the sub-6 GHz link when the mmWave connection becomes unusable. However, the microwave radio capacity is significantly lower as compared to that of the mmWave radio, thus implying that the practical gains of using microwave systems as a backup option may be limited. This is particularly true for bandwidth-hungry applications with stringent throughput requirements that are envisioned for mmWave-based NR systems [13], [4].

In this work, we aim to quantify the performance of multi-band 5G NR deployments in the microwave and mmWave bands. Particularly, we focus on characterizing the gains of employing microwave systems for improved 5G NR session continuity in applications with strict throughput requirements as well as studying the impact of mmWave-based NR traffic on sub-6 GHz BS service. As key performance indicators (KPIs) for our setup, we consider (i) new and (ii) ongoing mmWave session drop probability, (iii) microwave session drop probability, as well as (iv) radio resource utilization in mmWave and microwave systems.

To achieve the above objective, we integrate the tools of

[1]https://www.ericsson.com/en/press-releases/2017/12/global-mobile-industry-leaders-achieve-multi-band-5g-nr-interoperability

queuing theory and stochastic geometry with a realistic 3GPP cluster-based radio propagation model. Subsequently, we construct a novel framework capable of capturing both resource allocation and rerouting dynamics between the microwave and the mmWave BSs as well as the wireless aspects of the microwave and mmWave systems, including multi-path propagation, link blockage, and directional antenna patterns. The main contributions of our study that expand the state-of-the-art knowledge are:

- Mathematical framework that allows to capture the dynamics of the resource allocation in multi-band microwave/mmWave systems under dynamic blockage conditions;
- Offloading mmWave sessions with strict throughput requirements onto microwave links during service outage intervals leads to a resource capture effect by the "heavy-weight" mmWave sessions. This functionality decreases the resource utilization in microwave systems and at the same time negatively affects the new session drop probability;
- The impact of dual-band operation on the applications with stringent throughput requirements is moderate and the ongoing mmWave session drop probability remains considerably high. Hence, dual-band operation must be complemented with other mechanisms that improve the session continuity in mmWave 5G NR systems, such as mmWave band multi-connectivity operation.

The rest of this text is organized as follows. In Section II, we offer an overview of recent work related to the session continuity analysis in 5G NR. In Section III, we introduce our system model and its main components. The performance evaluation framework is developed in Sections IV and V. Numerical results are discussed in Section VI. Conclusions are stated in the last section.

II. Session Continuity in mmWave NR Systems

The link blockage and its statistical properties have been deeply investigated thus far. Notably, the authors in [6], [14] reported that the attenuation caused by human-body blockage resides in the range of 10 to 30 dB. Analytical models for static environments have been proposed in [15], [16] by showing that the blockage probability scales as a power function of the blocker intensity. The dynamic blockage of propagation paths in mmWave NR systems has been thoroughly studied in recent literature. In [7], the authors considered the case of static UE and moving blockers by demonstrating that the mean durations of the line-of-sight (LoS) blocked and LoS non-blocked intervals are on the order of hundreds of milliseconds. Similar durations have been reported in [17] for the case of static blockers and moving UE.

To mitigate the problem of blockage-induced outages, mmWave-specific solutions include the ratified *multi-connectivity* functionality, *resource reservation* at the BSs, and *multi-band* operation. The former option relies on the macro-diversity of the mmWave transmissions by allowing the establishment of multiple concurrent radio links with the BSs in proximity. In the case of an outage, the UE connection may transfer to one of the backup links. To improve the session continuity in early roll-outs of mmWave NR systems, a bandwidth reservation technique was introduced in [18]. Accordingly, a certain fraction of radio resources is only made available for the sessions that have already been accepted for service by the system. The performance of this method was assessed in [19], where the authors showed that the latter might effectively balance the ongoing session drop probability and the new session drop probability. A combined use of multi-connectivity and bandwidth reservation options was evaluated in [11], where it was demonstrated that enforcing mmWave NR BS selection at the connection establishment phase improves the session continuity.

Another approach to enhancing the session continuity in early-stage 5G NR deployments is to utilize the conventional LTE system. The authors considered in [20] the provisioning of emergency high-rate services in urban conditions. The dynamic blockage events caused by vehicles moving along the road lead to outage situations for the mmWave service, and the LTE infrastructure may be employed as a backup option. The authors confirmed that even though LTE allows for much-improved performance of emergency services, the resultant effect on the operation of LTE sessions is substantial. Most of the ongoing sessions accepted for service by the LTE BS are disadvantaged due to repeated outages experienced by the emergency services at the mmWave BSs. Further, the LTE system remains severely underutilized. The main reason for these effects is a mismatch in the data rate between the two technologies.

The work in [21] further considered multi-band connectivity performance (mmWave and sub-6 GHz NR) by relying upon a real-world deployment at the Lancaster University campus. However, those experimental results were not supported by theoretical models; hence, they are limited to that specific scenario. The authors in [22] formulated a multi-band switching task between the microwave and the mmWave systems as an optimization problem by targeting the maximization of the minimum user throughput in the system. The formulation in question has been further transformed into a more straightforward mixed integer programming problem and solved using standard numerical optimization methods. The reported results have argued for enhanced user throughput. However, as the BS resource allocation aspects were left outside of that study, the quality of service provisioning via optimized sub-6 GHz BS allocation and subsequent load balancing remain unclear. By aiming to improve the outage probability, the authors of [23] considered a joint operation of the microwave and mmWave systems and proposed a new connectivity mechanism that enhances the SINR coverage. They also assessed the BS density required to maintain the outage probability below a certain level.

Overall, multi-band operation is considered to be an important mechanism for improving the session continuity. The existing studies address the mmWave NR and microwave (NR or LTE) multi-band performance by considering static network conditions under elastic traffic demands with the tools of stochastic geometry. However, emerging mmWave NR deployments that have larger capacity at their disposal primarily

TABLE I
NOTATIONS USED IN THIS PAPER.

Notation	Description
N	Number of mmWave BSs covered by a sub-6 GHz BS
R_i	Bandwidth of sub-6 GHz BS and mmWave BS i
f_{NR}, f_L	mmWave and sub-6 GHz carrier frequency
h_L, h_{NR}, h_U	Height of sub-6 GHz BS, mmWave BS, and UE
r_B, h_B	Blocker radius and height
λ_B	Density of blockers
v_B, τ_B^{-1}	Blocker speed and mean movement time
λ_i	Session arrival intensity at BS i
μ_L^{-1}, μ_{NR}^{-1}	Service time of sub-6 GHz and mmWave sessions
c_i	Requested data rate at BS i
f_j^i,	pmfs of session resource requirements at BS i
φ_i	Rerouted session intensity to BS i
α	Session state change intensity caused by blockage
π_r	Probability of rerouted session returning back to mmWave
K_i	Maximum number of sessions at BS i
$B(x)$	CDF of service time for rerouted sessions
b	Mean service time for rerouted sessions at node N
$q_{n_1,n_2}(r_1, r_2)$	Stationary probabilities of the queuing model
$\pi_{N,i}$	New session drop probability at BS i
π_N	Averaged new session drop probability at mmWave BSs
U_i	Radio resource utilization at BS i
$U_{N,r}$	Sub-6 GHz resource occupied by rerouted sessions
$\pi_{T,i}$	Session drop probability upon return to mmWave BS
$\pi_{O,i}$	Probability of NR session drop at sub-6 GHz BS
π_O	Probability of an ongoing session drop
$\pi_{O\|N}$	Probability of mmWave session drop at sub-6 GHz BS
$P_{T,N}, P_{T,L}$	mmWave BS and sub-6 GHz BS transmit power
$G_{B,N}, G_{U,N}$	mmWave BS and mmWave UE gains
$G_{B,L}, G_{U,L}$	sub-6 GHz BS and sub-6 GHz UE gains
$S_B, M_{S,B}$	Shadow fading in blocked state and its margin
I, M_I	Interference and interference margin
N_0	Thermal noise
ζ_{NR}, ζ_L	mmWave and sub-6 GHz path loss exponents
C_L	Cable losses
W	Number of clusters in 3D mmWave propagation model
$w_{B,i}, w_{B,i}$	Width and length of cluster i blockage zone
$p_{B,i}(x)$	Blockage probability of i-th cluster at distance x
$P_{s,n}$	Fraction of power of cluster i
$P_n(x)$	Received power at distance x of cluster n
P_R	Received power at mmWave UE
$P_R^\star$	Conditional received power at mmWave UE
$\theta_i(x)$	Zenith of arrival for cluster i
$\theta_{3dB}^{\pm}$	3-dB point of the antenna array
$p_{O,1}(x)$	Outage probability at distance x due to blockage
$p_{O,2}(x)$	Outage probability at distance x due to insufficient power
$p_O(x)$	Overall outage probability at distance x
S_T	Outage power threshold
S_{min}	SNR outage threshold corresponding to the lowest MCS
r_{NR}, r_L	Coverage range of mmWave BS and sub-6 GHz BS
p_C	NR BS cell-edge coverage probability
$L_{dB}(x)$	Path loss at distance x in dB
G	Mean antenna gain over HPBW
J	Number of antenna elements
s_i, m_i	SNR margin and MCS i selection probability
S_L	SNR with sub-6 GHz BS
O, T	Outage and non-outage intervals
$B_i, B_i^\star$	Blockage and non-blockage intervals for cluster i
$\epsilon_i(x)$	Intensity of blockers crossing the blockage zone
$\eta_i(x, y)$	Movement angles in the blockage zone for cluster i
I_n	Indicator function for cluster n availability
$q_{O,n}$	Cluster n outage probability
$(\vec{\rho}, S)$	Parameters of phase-type distribution
$S_i(t)$	Absorbing Markov chain ($t \geq 0$)
T_i	Non-outage interval for cluster i

target bandwidth-hungry applications with more stringent data rate requirements [13], [4]. We aim to evaluate the performance of such services by taking advantage of multi-band mmWave and microwave NR capabilities under dynamic link blockage situations. To the best of our knowledge, there have been no analytical frameworks proposed to date for assessing the impact of multi-band operation on session continuity.

III. PROPOSED SYSTEM MODEL

This section introduces the considered multi-band scenario and outlines the associated system model by specifying its components including the deployment, mmWave and microwave propagation properties, link blockage, antenna configuration, radio connectivity, resource allocation, and session rerouting models. We also define the metrics of interest. The modeling parameters are provided in Table I.

A. Deployment Model

We consider the deployment of mmWave BSs within the coverage area of a single microwave[2] cell as demonstrated in Fig. 1. We assume that there are $N-1$ mmWave BSs enumerated as $1, 2, \ldots, N-1$ inside the coverage area of a single sub-6 GHz BS indexed by N (only one is shown in Fig. 1). The heights of sub-6 GHz and mmWave BSs are assumed to be h_L and h_{NR}, respectively. We note that the deployments of mmWave BSs may have different densities, which reflect various 5G NR market penetration phases.

We assume that sub-6 GHz and mmWave cell coverage ranges are circular with radii r_L and r_{NR}, respectively. In practice, these are heavily affected by large-scale objects in the environment. However, our model may capture practical coverage, e.g., available via field measurements. Microwave and mmWave BSs operate over a set of bandwidths R_N and R_i, $i = 1, 2, \ldots, N-1$, correspondingly.

B. Propagation and Blockage Models

To characterize the outage dynamics in 5G NR systems, we rely upon a fine-grained cluster-based multi-path propagation model that was ratified by 3GPP in [24]. Accordingly, the full received power comprises the contributions from LoS and reflected components. This model binds the features of the propagation environment to a finite set of parameters, including (i) zenith of arrival and departure angles (ZOA, ZOD) and azimuth angles of arrival and departure (AOA, AOD) of clusters, (ii) associated cluster delay, and (iii) power fraction of a cluster.

Even though the model in question is algorithmic, which offers no closed-form expression for AOA, ZOA, and receiver power, the authors in [25] demonstrated that (i) ZOA $\theta_i(x)$ of cluster i, $i = 1, 2, \ldots, W$, can be closely approximated by a Laplace distribution, with the mean coinciding with the zenith and azimuth angles of LoS path and constant variance and (ii) received power of cluster i follows a Log-Normal distribution, i.e.,

$$f_{\theta_i}(y; x) = \frac{1}{2a_{i,2}(x)} e^{-\frac{|y - a_{i,1}(x)|}{a_{i,2}(x)}}, \; f_{P_{S,i}}(y; x) = \\ = \frac{1}{y a_{i,4}\sqrt{2\pi}} e^{-\frac{(\ln y - a_{i,3})^2}{2a_{i,4}^2}}, \; i = 1, 2, \ldots, W, \quad (1)$$

where $a_{i,1}(x)$, $a_{i,2}(x)$, $a_{i,3}(x)$, and $a_{i,4}(x)$ are the parameters estimated from statistical data [25].

We also assume that a human body can occlude a multi-path component in a dynamic crowd. Humans are modeled by cylinders with the base radius r_B and the constant height h_B. The density of blockers in the environment is λ_B. Blockers are allowed to move in $\Re^2$ according to the random direction

[2]Even though microwave BSs may operate based on NR or LTE technology, we consider sub-6 GHz NR as an example.

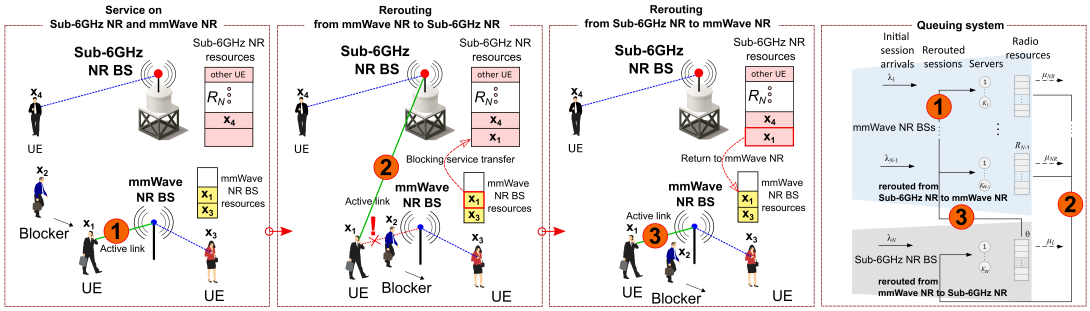

Fig. 1. Illustration of considered multi-band (sub-6 GHz and mmWave) deployment with multiconnectivity capabilities.

model (RDM, [26]). The flux of blockers across the cell boundaries is assumed to be constant, that is, the blockage environment is homogeneous.

The path loss for the sub-6 GHz radio is given by [24]

$$L_{dB}(x) = 32.4 + 21\log(x) + 20\log f_L, \tag{2}$$

where f_L is the carrier frequency in GHz and x is the distance.

Microwave systems are considerably less affected by human-body blockage, and the induced attenuation is reported to be not more than 2-4 dB [27]. Hence, UEs seldom experience outage conditions in these systems should the currently dominant propagation path be occluded.

C. Antenna Models

We assume planar antenna arrays at both the BS and the UE. Similarly to [28], we utilize a cone model with the beamwidth corresponding to half-power beamwidth (HPBW) of the antenna radiation pattern. Using [29], the mean antenna gain over HPBW is given by

$$G = \frac{1}{\theta^{+}_{3db} - \theta^{-}_{3db}} \int_{\theta^{-}_{3db}}^{\theta^{+}_{3db}} \frac{\sin(J\pi\cos(\theta)/2)}{\sin(\pi\cos(\theta)/2)} d\theta, \tag{3}$$

where J is the number of antenna elements.

The HPBW of the array, α, can be determined as $\alpha = 2|\theta_m - \theta^{\pm}_{3db}|$, where θ_m is the array maximum that can be computed as $\theta_m = \arccos(-1/\pi)$, $\theta^{\pm}_{3db}$ are the upper and lower 3-dB points estimated as $\theta^{\pm}_{3db} = \arccos[-\pm 2.782/(J\pi)]$. For practical calculations, we employ the HPBW approximation given by $102/J$, where J is the number of antenna arrays in the appropriate plane [30]. Similarly, the linear gain can be approximated by the number of elements [29].

D. Traffic Model

We consider two types of UEs. The first one supports both sub-6 GHz and mmWave technologies, while the second one is restricted to sub-6 GHz radio only. Accordingly, we assume that the process of new session arrivals to a mmWave BS i is homogeneous Poisson having the intensity λ_i, $i = 1, 2, \ldots, N-1$. These sessions are generated by multi-band UEs. The geometric locations of these sessions are required to be distributed uniformly within the respective coverage areas of mmWave BSs. The service time of a session is assumed to be distributed exponentially with parameter μ_{NR}. A session arriving to mmWave BS i requests constant bitrate c_i. The process of new session arrivals to sub-6 GHz radio is homogeneous Poisson having the intensity of λ_N. Single-band UEs generate these sessions. The service time is distributed exponentially with the parameter μ_L. A session arriving to the sub-6 GHz BS requests constant bitrate c_N.

Using the radio system parameters, the NR modulation and coding schemes (MCSs, [31]), and the distance from the active UE to the microwave and mmWave BSs, the requested data rates c_N and c_i are translated into the probability mass function (pmf) of the radio resources at the microwave and mmWave air interfaces, f^i_j, $i = 1, 2, \ldots, N$, $j \geq 0$ in Section IV. Note that multi-band UEs are characterized by different resource requirements when served at sub-6 GHz vs. mmWave BSs. We denote the pmf of session resource requirements for multi-band UEs at sub-6 GHz BS by f^N_j, $i = 1, 2, \ldots, N-1$, $j \geq 0$.

E. Multi-Band Connectivity and Resource Allocation

We assume that sessions generated by single-band UEs request service exclusively from the sub-6 GHz BS, while those initiated by multi-band UEs always request service from the mmWave BSs, see Fig. 1. Multi-band UEs are assumed to maintain simultaneous connections to sub-6 GHz and mmWave BSs.

A session arriving at mmWave BS i requests a certain amount of radio resources with the pmf f^i_j, $i = 1, 2, \ldots, N-1$, $j \geq 0$. It is accepted for service if there is a sufficient volume of radio resources available at the time of its arrival (point 1 in Fig. 1). Otherwise, the session is dropped upon arrival. During the session service time at its mmWave BS, a multi-band UE may experience outage conditions. In this case, a session is immediately transferred to a sub-6 GHz BS, where it requests resources with the pmf f^N_j (point 2 in Fig. 1).

If there are insufficient available resources at the sub-6 GHz BS, the session is dropped. Otherwise, it is accepted by the sub-6 GHz BS for the duration of the outage situation on the mmWave link. Upon entering a non-outage state with the mmWave BS, the session is immediately rerouted back, where it requests the amount of resources with the pmf f^i_j and may again be dropped due to the unavailability of the demanded resources (point 2 in Fig. 1).

Each active session during its service at the mmWave BS is associated with a homogeneous Poisson process of the UE state changes with the intensity α. Upon a state change from non-outage to outage conditions, the session is rerouted to the sub-6 GHz BS N with its new resource demands being distributed according to the pmf f^N_j, $j \geq 0$. The same access

rules apply at this stage: if there are insufficient available resources at the sub-6 GHz BS N, the session is dropped.

Rerouted sessions arriving to the sub-6 GHz BS are assumed to form a Poisson process[3] with the intensity φ_N. Rerouted sessions depart from the sub-6 GHz BS N either upon a service completion or due to a change in the UE state from outage to non-outage conditions at mmWave BSs. The mean values of the outage and non-outage intervals are estimated in Section IV. If the residual service time exceeds the time spent at the sub-6 GHz BS N, the session returns to its original mmWave BS, provided that it passes the same access rules with the original pmf of the resource requirements f_j^i, $j \geq 0$. Similarly to sessions returning to sub-6 GHz BS, we assume that the sessions returning to the mmWave BS i form a Poisson process with the intensity φ_i.

It is further assumed that sub-6 GHz coverage is provisioned such that no outage occurs during a session lifetime in the system. Hence, a session generated by a single-band UE can only be dropped upon its arrival if there are insufficient radio resources available at the sub-6 GHz BS. Observe that there are no priorities offered to either single- or multi-band UEs at the sub-6 GHz BS, and they fairly compete for the available resources.

F. Metrics of Interest and Solution Outline

In the rest of this work, we consider the following KPIs: (i) new mmWave session drop probability, i.e., the probability that a session of a multi-band UE is not accepted for service due to resource unavailability at the mmWave BS, (ii) ongoing mmWave session drop probability, i.e., the probability that a session of a multi-band UE, which was accepted for service, is then dropped during service at either mmWave or sub-6 GHz BS due to rerouting, (iii) new sub-6 GHz session drop probability, i.e., the probability that a session of a single-band UE is not accepted for service due to resource unavailability at the sub-6 GHz BS, and (iv) average amount of radio resources occupied at the sub-6 GHz and mmWave BSs. The framework developed in what follows allows for estimating these metrics as functions of the input system parameters.

To derive the metrics of interest, we develop the following two-stage performance evaluation framework. First, to account for the specifics of the considered environment and the NR interface parameters, we derive the pmfs of the radio resource requirements by a single session, f_j^i, $i = 1, 2, \ldots, N$, $j \geq 0$, f_j^N, $j \geq 0$, the intensity of the UE state changes α, and the CDF of the outage time, $F_T(x)$, $x > 0$ in Section IV. These parameters are utilized further in Section V to specify the queuing model that captures the nature of the service procedure in the considered multi-band NR environment. We note that these two stages are easily separable by implying that the developed queuing model can be utilized as a standalone method to capture various deployment scenarios that include multi-band operation.

[3]In fact, the flows returning to the mmWave BSs $1, 2, \ldots, N-1$ are not Poisson in nature. However, as we demonstrate later in Section VI, the adopted assumption does not degrade the modeling accuracy.

On top of the introduced assumptions, our analysis utilizes the following approximations and/or considerations: (i) state aggregation technique, (ii) Poisson assumption for the rerouting traffic intensity, and (iii) iterative solution algorithm. In Section VI, when producing the numerical results, we first assess the accuracy of the developed framework by comparing its output to that of the simulations.

Our proposed methodology is tailored to the session-level analysis of the mmWave NR BSs, where one has to ensure that the traffic load does not exceed the system capacity in the long run. Local fluctuations in the user demand are assumed to be handled at the lower layers by taking advantage of buffering, scheduling, and radio-level mechanisms, such as beamforming, beamsteering, and power control. Hence, we focus on the capability of the mmWave-based NR BSs with multi-band operation to handle their offered load. Particularly, our developed framework allows for determining how many sessions might be supported by the NR BS with multi-band operation. The answer is not straightforward as the amounts of resources that need to be provided in the long run for each individual session heavily depend on the UE location. Recalling that the session arrival patterns, their service times, and data rate requirements may also be random, to determine the system capacity in terms of the supported intensity of sessions with desired drop margins, one has to utilize the tools of queuing theory.

IV. Model Parametrization

In this section, by following our methodology we derive the parameters characterizing the propagation and environmental characteristics. Particularly, we determine the pmfs of the radio resource requirements, f_j^i, $i = 1, 2, \ldots, N$, $j \geq 0$, f_j^N, $j \geq 0$, the intensity of the UE state changes α, and the CDF of the outage time, $F_T(x)$, $x > 0$.

All the pmfs of the amount of requested resources are obtained similarly for all the mmWave BSs. As an example, we consider the pmfs f_j^i, $i = 1, 2, \ldots, N$, $j \geq 0$. To obtain them for a randomly chosen mmWave BS i, one needs to determine the consecutive coverage area of the mmWave BS, link blockage probability, outage probability, probability density function of SNR conditioned on the event that the UE resides in non-outage conditions. Further, one has to discretize it according to the 5G NR MCSs [31], and then scale the result with the session data rate c_i.

A. Outage Probability with mmWave BS

Denote by $p_{B,i}(x)$, $i = 1, 2, \ldots, W$ the blockage probability of cluster i. We start with the LoS path corresponding to $p_{B,1}(x)$. Similarly to [16], we specify the LoS blockage zone associated with the UE. The width and length of this zone are

$$w_{B,1} = 2r_B,\, l_{B,1} = \left(x \frac{h_B - h_U}{h_{NR} - h_U} + r_B \right), \qquad (4)$$

where r_B is blocker radius, x is 2D distance.

Since geometric locations of blockers are distributed uniformly within the mmWave BS coverage, and using the void

probability of a Poisson point process (PPP), the probability of the LoS path blockage is given by

$$p_{B,1}(x) = 1 - e^{-2r_B\lambda_B\left[x\frac{h_B-h_U}{h_{NR}-h_U}+r_B\right]}. \quad (5)$$

Consider further i-th cluster blockage probability, $p_{B,i}$, $i = 2, 3, \ldots$. Similarly to the LoS cluster, for any given ZOA y_i of cluster i, $i = 2, 3, \ldots, N$, we determine cluster i blockage zone. Hence, for cluster i, the blockage probability is

$$p_{B,i}(y; x) = 1 - e^{-2\lambda_B r_B(\tan y_i(h_B-h_U)+r_B)}. \quad (6)$$

Accounting for the pdf of ZOA θ_i provided in (1), we obtain

$$p_{B,i}(x) = \int_{-\pi}^{\pi} f_{\theta_i}(y; x)p_{B,i}(y; x)dy, \quad (7)$$

which can be estimated by numerical integration.

The power of each cluster can thus be written as

$$P_n(x) = P_{s,n}10^{(P_{T,N}-L_{dB}(x))/10},\ n = 1, 2, \ldots, W, \quad (8)$$

where $L_{dB}(x)$ is the path loss and $P_{T,N}$ is the transmit power. Applying the 3GPP UMi LoS path loss model in (8), we have

$$P_n(x) = P_{s,n}10^{(P_{T,N}-32.4-20\log_{10} f_{NR}-21\log_{10} x)/10}. \quad (9)$$

The pdf of cluster power can be found by utilizing the transformation technique for a random variable (RV) [32]

$$f_{P_n}(z; x) = \frac{f_{P_{s,n}}\left(\frac{P_n(x)}{10^{(P_{T,N}-32.4-20\log_{10} f_{NR}-21\log_{10} x)/10}}\right)}{10^{(P_{T,N}-32.4-20\log_{10} f_{NR}-21\log_{10} x)/10}}. \quad (10)$$

The pdf of the strongest cluster is obtained by weighting

$$f_{P_R}(z; x) = \sum_{i=1}^{W}\left[(1 - p_{B,i}(x))\prod_{j=1}^{i-1} p_j(x)\right] f_{P_n}(z; x). \quad (11)$$

One can now determine the outage probability. The outage is experienced at the UE when either of the following events occurs: (i) all clusters are blocked simultaneously, (ii) the received power of the strongest clusters is below the threshold S_T. The corresponding outage probabilities for these cases are

$$p_{O,1}(x) = \prod_{i=1}^{N} p_{B,i}(x),\ p_{O,2}(x) = \int_0^{S_T} f_{P_R}(z; x)dz. \quad (12)$$

The outage probability is then given by

$$p_O(x) = \prod_{i=1}^{N} p_{B,i}(x) + \int_0^{S_T} f_{P_R}(z; x)dz. \quad (13)$$

B. Resource Demands at BSs

To determine the SNR pdf, one needs to obtain the coverage radius of a single mmWave BS. Using the outage threshold S_T and applying the UMi Street-Canyon mmWave propagation model [24], we may write

$$S_T = \frac{P_{T,N}G_{B,N}G_{U,N}}{N_0C_LIS_B(r_{NR} + [h_{NR} - h_U]^2)^{\zeta_{NR}/2}}, \quad (14)$$

where ζ_{NR} is the path loss exponent, h_{NR}, h_U are the mmWave BS and UE heights, $P_{T,N}$ is the mmWave BS transmit power, $G_{B,N}$, $G_{U,N}$ are the mmWave BS and UE antenna gains, N_0 is the noise, C_L is the cable losses, I is the interference, and S_B is the shadow fading.

Observe that S_T is a function of two RVs, I and S_B. To simplify calculations and at the same time provide an adequate approximation for r_i, we capture both the shadow fading in the LoS blocked state and the interference from the adjacent mmWave BSs using the shadow fading margin $M_{S,B}$ and the interference margin M_I, respectively, as provided in [24]. However, one may estimate them precisely by using stochastic geometry tools [33], [28].

Solving (14) with respect to r_{NR}, we establish

$$r_{NR} = \sqrt{\left(\frac{P_{T,N}G_{B,N}G_{U,N}}{N_0C_LM_IM_{S,B}S_T}\right)^{\frac{\zeta_{NR}}{2}} + (h_{NR} - h_U)^2}, \quad (15)$$

where $M_{S,B}$ is calculated as $M_{S,B} = \sqrt{2}\sigma_{S,B}\text{erfc}^{-1}(2p_C)$, $\text{erfc}^{-1}(\cdot)$ is the inverse complementary error function, p_C is the mmWave BS cell-edge coverage probability, and $\sigma_{S,B}$ is the standard deviation (STD) of shadow fading for the LoS blocked state as provided in [24].

The conditional pdf of the received power at distance x is

$$f_{P_R^\star}(z; x) = \frac{\sum_{i=1}^{W}\left[[1 - p_{B,i}(x)]\prod_{j=1}^{i-1} p_j(x)\right] f_{P_n}(z; x)}{1 - p_O(x)}. \quad (16)$$

Accounting for random locations of active UEs within the mmWave BS coverage, the SNR pdf of a randomly selected UE is given by

$$f_{P_R^\star}(z) = \int_0^{r_{NR}} f_{P_R^\star}(z; x)\frac{2x}{r_{NR}^2}dx, \quad (17)$$

which is used to determine the outage probability.

Let the SNR margins of the mmWave MCSs [31] be s_i, $i = 1, 2, \ldots$. Denoting the probability of selecting MCS i by m_i, we arrive at

$$m_i = Pr\{s_i < s < s_{i+1}\} = F_S(s_{i+1}) - F_s(s_i). \quad (18)$$

Once m_i, $i = 1, 2, \ldots$, are obtained, the amount of radio resources required by a session follows.

Due to a different structure of the sub-6 GHz propagation model, the derivation of pdf of the radio resource requirements is simpler. Let S_L be the RV denoting the SNR with sub-6 GHz BS and $F_{S_L}(x), x > 0$, be its CDF. Recall that the locations of new session arrivals are assumed to be distributed uniformly within the sub-6 GHz BS coverage. Hence, the CDF of distance between the UE and the BS reads as

$$F(y) = (y^2 - (h_L - h_U)^2)/r_L^2, \quad (19)$$

where r_L is the coverage range of the sub-6 GHz BS.

Finally, the SNR CDF can be expressed as

$$F_{S_L}(y) = 1 - F(P_{T,L}G_{B,L}G_{U,L}/N_0A_Ly^{\zeta_L/2}), \quad (20)$$

and the rest of the procedure is similar to the case of mmWave NR.

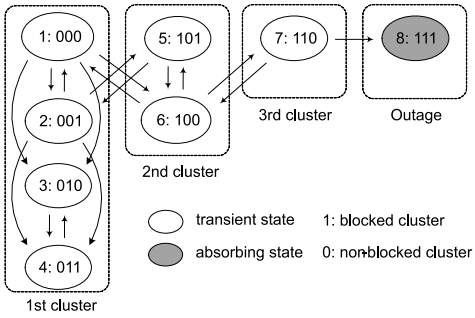

Fig. 2. Absorbing Markov chain capturing time to outage for $W = 3$.

C. Intensity of State Changes

We continue by obtaining the intensity of UE state changes, α, between outage and non-outage conditions when associated with the mmWave BS. Similarly to the intensity of blockage and non-blockage state changes addressed in [7], one may deduce that the case of interest is an alternating renewal process with outage, O, and non-outage, T, periods that have different distributions. We approximate α as $\alpha = 2/(E[T] + E[O])$, where both $E[T]$ and $E[O]$ are the unknowns to be determined in what follows.

Observe that the outage probability in (13) can be interpreted as a fraction of time that the UE spends in outage conditions, i.e., $p_O = E[O]/(E[T] + E[O])$. Since

$$E[O] = \frac{E[T] + p_O E[T]}{p_O}, \tag{21}$$

it is sufficient to obtain $E[T]$ to determine α.

Recall that in our model, a UE always experiences outage conditions when all of its multi-path components are blocked and may also observe outage when a certain path is not blocked but the SNR falls below a particular threshold. Further, we first determine the time intervals related to blockage of all the multi-path components and then build a model that accounts for outage caused by the SNR variations.

Consider the blockage zone corresponding to cluster i. Let B_i and $B_i^\star$ denote blockage and non-blockage periods. Following [34], the intensity of blockers crossing the blockage zone of the UE is given by

$$\epsilon_i(x) = \frac{\lambda_B e^{-1/\tau_B}}{2\pi} \sum_{i=1}^{7} \iint_{M_i} \eta_i(x,y)\, dx\, dy, \tag{22}$$

where τ_B^{-1} is the mean length of the RDM run, M_i is the area of zone i, $\eta_i(x,y)$ is the movement angle ranges in zone i that result in entering the LoS blockage zone, and λ_B is the intensity of blockers. The mean intensity of blockers crossing the LoS blockage zone is thus

$$\epsilon_i = \int_0^{r_{NR}} \epsilon_i(x) \frac{2x}{r_{NR}^2} dx. \tag{23}$$

It has been shown in [7] that the duration of the blocked phase can be modeled by the busy period of M/G/∞ queue. The latter can be obtained numerically by using the mean blockage zone residence time, L, via, e.g., [35]. The distribution of L can be produced similarly to [7]. Taking one step further and approximating M/G/∞ by M/M/∞ with the coinciding mean service time, the mean durations of non-blockage and blockage periods are provided by

$$E[B_i^\star] = 1/\epsilon_i,\ E[B_i] = \frac{1}{\epsilon_i} \sum_{i=1}^{\infty} (\epsilon_i E[L])^i. \tag{24}$$

D. Distribution of Outage Time

It is assumed that a UE operates over the mmWave band by using the most powerful cluster. Further, even when W clusters are available, for a particular UE only a subset of those may have the SNR level of above the reception threshold S_T. The probability that cluster n experiences outage is given by

$$q_{O,n} = \int_0^{r_{NR}} \frac{2x}{r_{NR}^2} \int_{S_T}^{\infty} f_{P_n}(z;x) dx, \tag{25}$$

where $f_{P_n}(z;x)$ is the pdf of cluster n as per (10).

Let I_n be the indicator function of cluster n availability, i.e., $I_n = 1$ when cluster n has insufficient SNR and $I_n = 0$ when the SNR is higher than S_T. Consider now the case where i out of M clusters are in non-outage conditions since the SNR is higher than S_T. There are $2^W - 1$ such combinations in total. Observe that a particular combination can be written in a binary form, e.g., 101 for $W = 3$, thus implying that the first and third strongest clusters experience outage as a result of insufficient SNR, which leaves only the second cluster available for the UE. We denote the probability of each combination by w_i, $i = 1, 2, \ldots, 2^W - 1$. They can be obtained directly, e.g., the probability of 101 for $W = 3$ is $q_{O,1}(1 - q_{O,2})q_{O,3}$.

To characterize the outage process, for each feasible combination of the available clusters, we specify an absorbing Markov model $\{S_i(t), t \geq 0\}$ that represents the process of cluster blockage defined over the state space $S_i(t) \in \{1, 2, \ldots, 2^W\}$. An example state transition diagram of the process for $W = 3$ is illustrated in Fig. 2. The state 111, where all the clusters are blocked, is considered to be absorbing. The intensities of transitions between the states are provided by $1/E[B_i]$ and $1/E[B_i^\star]$, where $E[B_i]$ and $E[B_i^\star]$ are the means of blockage and non-blockage intervals for cluster i.

The distribution of time until outage in $\{S_i(t), t \geq 0\}$ is of phase-type with the representation $(\vec{\rho}, S)$, where ρ is the initial state distribution at $t = 0$ defined over $\{1, 2, \ldots, 2^W - 1\}$ and S is the rate matrix obtained from the infinitesimal generator by excluding the first row and the first column. The sought pdf of the outage time is [36]

$$f_{T_i}(t) = \vec{\rho} e^{St} \vec{s}_0,\ t > 0, \tag{26}$$

where $\vec{s}_0 = -S\vec{1}$, $\vec{1}$ is the vector of ones of size $1 \times 2^W - 1$, and e^{St} is the matrix exponential. The initial state probability vector ρ is derived from the steady-state distribution of the Markov chain with all recurrent states. Once the non-outage periods $E[T_i]$ are obtained, the mean non-outage period is provided by weighting $E[T_i]$ with the corresponding probabilities. By substituting it into (21), we establish the mean outage period $E[O]$ and then the mean intensity of the UE state changes, α.

V. Performance Evaluation Framework

In this section, our performance evaluation framework is detailed. Using the pmf of the radio resource requirements and the outage intensity as input, we formulate a queuing model describing single- and multi-band UE service processes at the NR BSs. We then proceed by describing the solution methodology and estimating the performance metrics.

A. Queuing Network Formalism and Solution

The session service model specified in subsection III-E is a special case of the queuing network with random resource requirements. As one may observe, there is a dependency between the service processes at the BSs constituting the network. This aspect prohibits from the use of conventional Markov chain methods. As a result of random resource requirements, a complete description of the system requires an infinite-dimensional stochastic process. Here, to properly release the resources at the time of session departure, one needs to track the amount of radio resources requested by each session upon its arrival and rerouting. These two properties do not allow for solving the system at hand directly.

We follow the decomposition approach to address this model, which is a powerful methodology for queuing networks [37]. The core assumption here is that the service process at each BS in the network is independent of the service processes at other nodes. The interdependence between the mmWave BS service processes is incorporated into the numerical solution algorithm, where the characteristics of the entire system are recalculated recursively at each step until the procedure converges. The stability properties of this class of models were analyzed in [38]. Following our core assumption, the service processes at the BSs are assessed in isolation by updating the intensity of flows between them. To further reduce the complexity of such analysis, we employ the state aggregation technique [39].

B. Service Dynamics at mmWave BSs

First, consider the mmWave BS i. Due to the memoryless property, the residual service time of returning sessions is exponential with the parameter μ_{NR}. The total session arrival intensity to node i is thus $\lambda_i + \varphi_i$ and the total intensity of departures is $\mu_{NR} + \alpha$. Hence, the stochastic behavior of the mmWave BS i can be described by the Markov process $X_i(t) = \{\xi_i(t), \delta_i(t)\}$, where $\xi_i(t)$ is the number of sessions at time t and $\delta_i(t)$ is the total amount of occupied radio resources at time t. Denote the stationary probabilities $q_{i,n}(r)$ as

$$q_{i,n}(r) = \lim_{t\to\infty} P\{\xi_i(t) = n, \delta_i(t) = r\}, \quad n = 0, 1, 2 \ldots, K_i,\ r = 0, 1, 2 \ldots, R_i, \tag{27}$$

where K_i is the maximum number of sessions at the mmWave BS i.

The process $X_i(t)$ describes a queuing system with limited resources and random resource requirements [40]. According to [41], the stationary distribution of (27) is given by

$$q_{i,0} = \left(1 + \sum_{n=1}^{K_i} \frac{\rho_i^n}{n!} \sum_{r=0}^{R_i} f_r^{i,(n)}\right)^{-1}, \quad q_{i,n}(r) = q_{i,0} \frac{\rho_i^n}{n!} f_r^{i,(n)}, \quad n = 1, 2, \ldots, K_i, \tag{28}$$

where $\rho_i = (\lambda_i + \varphi_i)/(\mu_{NR} + \alpha)$ and $f_j^{i,(n)}, j \geq 0$ is the n-fold convolution of pmf $\{f_j^i\}, j \geq 0$. Note that the probability $f_r^{i,(n)}$ can be interpreted as the probability that n sessions completely occupy r resources at the mmWave BS i.

C. Service Dynamics at sub-6 GHz BS

The behavior of the sub-6 GHz BS can also be described in terms of the queuing systems with random resource requirements. However, in this case, there are two different types of sessions: those arriving from the single-band UEs and those rerouted from the mmWave BSs. The arrival intensity for the first type of sessions is λ_N and the service times are distributed exponentially with the parameter μ_L. On the other hand, the arrival intensity for the rerouted sessions is φ_N, which is obtained by summing up all the rerouting intensities of the mmWave BSs, $1, 2, \ldots, N-1$,

$$\varphi_N = \sum_{i=1}^{N-1} (\lambda_i + \varphi_i) \frac{\alpha}{\mu_{NR} + \alpha}. \tag{29}$$

In (29), the term $\alpha/(\mu_{NR}+\alpha)$ refers to the probability that a mmWave session is rerouted to the sub-6 GHz BS before its service completion. The intensities φ_i, $i = 1, 2, \ldots, N-1$, of the mmWave sessions returning from the sub-6 GHz BS to their original BS i, $1, 2, \ldots, N-1$ are

$$\varphi_i = (\lambda_i + \varphi_i)(1 - \pi_{N,i}) \frac{\alpha}{\alpha + \mu_{NR}} (1 - \pi_{N,N}) \pi_r, \tag{30}$$

where $\pi_{N,i}, i = 1, 2, \ldots, N$ is the new session drop probability at the mmWave BS i and π_r is the probability that a rerouted session at the sub-6 GHz BS N returns to its mmWave BS before service completion.

Importantly, (30) implies that the flow of rerouted sessions at the mmWave BS i equals the fraction of the accepted flow at the mmWave BS i, which was initially routed to the node N with the probability $\alpha/(\alpha + \mu_{NR})$, accepted by the node N with the probability $1 - \pi_{N,N}$, and finally rerouted back with the probability π_r. Here, π_r is the probability that the residual service time of a session exceeds the uninterrupted outage time with CDF $F_T(x)$ obtained in Section IV. Since these RVs are independent, we have

$$\pi_r = \iint_{x>y} \mu_{NR} e^{-\mu_{NR} x} d\left(F_T(y)\right) dx. \tag{31}$$

The service time of rerouted sessions at the sub-6 GHz BS is the minimum of the residual service time and the time to return to the original mmWave BS. Using the CDF of the

minimum of two RVs [32], we obtain the CDF $B(x)$ of the service time for the rerouted sessions as

$$B(x) = 1 - e^{-\mu_{NR}x}(1 - F_T(x)), \tag{32}$$

which leads to the mean service time at the node N as

$$b = \int_0^\infty e^{-\mu_{NR}x}(1 - F_T(x))dx. \tag{33}$$

The model of the sub-6 GHz BS i can also be classified as a queuing system with multiple customers and random resource requirements, which has been investigated in [42]. In [43], the authors demonstrated that the system's stationary distribution is insensitive to the type of service time distribution and only depends on its mean value. Using these results, the stationary probabilities $q_{n_1,n_2}(r_1, r_2)$ that n_1 sessions of the first type occupy r_1 resources and n_2 rerouted sessions occupy r_2 resources are provided by

$$q_{0,0} = \left(1 + \sum_{0<n_1+n_2\le K_N} \frac{\rho_{N,1}^{n_1}}{n_1!}\frac{\rho_{N,2}^{n_2}}{n_2!} \sum_{0<r_1+r_2\le R_N} f_{r_1}^{N,(n_1)} f_{r_2}^{N,(n_2)}\right)^{-1},$$

$$q_{n_1,n_2}(r_1, r_2) = q_{0,0}\frac{\rho_{N,1}^{n_1}}{n_1!}\frac{\rho_{N,2}^{n_2}}{n_2!} f_{r_1}^{N,(n_1)} f_{r_2}^{N,(n_2)}, \tag{34}$$

where $\rho_{N,1} = \frac{\lambda_N}{\mu_L}$ and $\rho_{N,2} = \varphi_N b$.

According to [39], the stationary probabilities (34) can be aggregated to probabilities $q_n(r)$ that n sessions completely occupy r resources as follows

$$q_n(r) = q_0\frac{\rho_N^n}{n!} f_r^{N,(n)},\ q_0 = \left(1 + \sum_{n=1}^{K_N}\frac{\rho_N^n}{n!}\sum_{r=0}^{R_N} f_r^{N,(n)}\right)^{-1},$$
$$\rho_N = \rho_{N,1} + \rho_{N,2}, \tag{35}$$

which can be estimated numerically, see, e.g., [44].

D. Solution and Performance Metrics

After obtaining the stationary state probabilities for all the BSs, we may proceed with deriving the identified performance metrics. Recall that our solution is iterative by nature as one needs to add another layer of rerouted sessions at each iteration until a parameter converges to its stable value with a given accuracy. The procedure is terminated once the required precision level is achieved. Particularly, at the first iteration, there are no rerouted sessions, and thus $\varphi_i = 0, i = 1; 2; ...; N-1$. Then, the algorithm continues as follows:

1) Based on λ_i, α, μ_L, μ_{NR}, π_r, b, and the pmfs of the resource requirements $\{f_j^i\}$, $i = 1, 2, ..., N$, new session drop probabilities $\pi_{N,i}$ at nodes $1, 2, ..., N-1$, arrival intensity of rerouted sessions φ_N, and new session drop probability $\pi_{N,N}$ at the node N are evaluated.
2) New values of φ_i are calculated according to (30) by substituting their previous values into the right-hand side; if the difference between the new and the previous value meets the required precision, the algorithm proceeds with 3). Otherwise, it returns to 1).
3) When φ_i converges to a stable value with the desired accuracy, all other performance metrics are evaluated.

The iterative solution outlined above requires new session drop probabilities. These can be obtained for the mmWave and sub-6 GHz sessions as follows

$$\pi_{N,i} = 1 - q_{i,0}\sum_{n=0}^{K_i-1}\frac{\rho_i^n}{n!}\sum_{r=0}^{R_i} f_r^{i,(n+1)},\ \pi_{N,N} =$$
$$= 1 - q_{N,0}\sum_{n=0}^{K_N-1}\frac{\rho_N^n}{n!}\sum_{r=0}^{R_N} f_r^{N,(n+1)}. \tag{36}$$

By averaging across all the mmWave BSs, we obtain the following expression for the new session drop probability

$$\pi_N = \left(\sum_{i=1}^{N-1}\lambda_i\right)^{-1}\sum_{i=1}^{N-1}\lambda_i\pi_{N,i}. \tag{37}$$

The resource utilization, U_i, is produced as

$$U_i = \frac{1}{R_i}q_{i,0}\sum_{n=0}^{K_i}\frac{\rho_i^n}{n!}\sum_{r=0}^{R_i} r f_r^{i,(n)}, i = 1, 2, \ldots, N. \tag{38}$$

The fraction of radio resources $U_{N,r}$ occupied by rerouted sessions at node N may be evaluated similarly by employing the stationary distribution (34), i.e.,

$$U_{N,r} = \frac{q_{0,0}}{R_N}\sum_{0<n_1+n_2\le K_N}\frac{\rho_{N,1}^{n_1}}{n_1!}\frac{\rho_{N,2}^{n_2}}{n_2!}\times$$
$$\times\sum_{0<r_1+r_2\le R_N} r_2 f_{r_1}^{N,(n_1)} f_{r_2}^{N,(n_2)}. \tag{39}$$

Calculation of the probability that an accepted mmWave session is dropped as a result of link blockage and a subsequent rerouting is a more involved process. Let us introduce the conditional probability $\pi_{T,i}$ that a session, which originally arrived at the mmWave BS i, is dropped during its ongoing service due to rerouting, i.e.,

$$\pi_{T,i} = \pi_{N,N} + (1 - \pi_{N,N})\pi_r\pi_{N,i}, \tag{40}$$

where the first term corresponds to the case of dropping the session at the sub-6 GHz BS N, while the second term is the probability that the rerouted session is accepted at the sub-6 GHz BS N but then dropped upon its return to the original mmWave BS due to insufficient resources.

The average number of sessions dropped as a result of insufficient radio resources at the sub-6 GHz BS during a time interval of length T is $\alpha\tilde{N}_i\pi_{T,i}T$, where $\tilde{N}_i$ is the mean number of sessions at node i. The mean number of sessions that are accepted during the same time interval is $\lambda_i(1-\pi_{N,i})$. Hence, the probability that a session, which was initially accepted at the mmWave BS i, was dropped is

$$\pi_{O,i} = \lim_{T\to\infty}\frac{\alpha\tilde{N}_i\pi_{T,i}T}{\lambda_i(1-\pi_{N,i})T} = \frac{\alpha\tilde{N}_i\pi_{T,i}}{\lambda_i(1-\pi_{N,i})}. \tag{41}$$

Averaging across all the mmWave BSs, we arrive at the following expression for the ongoing session drop probability

$$\pi_O = \left(\sum_{i=1}^{N-1}\lambda_i(1-\pi_{N,i})\right)^{-1}\sum_{i=1}^{N-1}\alpha\tilde{N}_i\pi_{T,i}. \tag{42}$$

Another parameter is the probability $\pi_{O,i|N}$ that a session drops as a result of its rerouting from node i to node N given

that it is eventually dropped. To derive $\pi_{O,i|N}$, one needs to represent the ongoing session drop probability $\pi_{O,i}$ in a way suitable for further manipulations. Observe that

$$\left[\frac{\alpha}{\alpha+\mu_{NR}}(1-\pi_{N,N})\pi_r(1-\pi_{N,i})\right]^k \frac{\alpha}{\alpha+\mu_{NR}}\pi_{N,N}, \quad (43)$$

which can be interpreted as the probability that a mmWave session is dropped during a reroute to the sub-6 GHz BS N after exactly k reroutes there and back.

Similarly, the probability that a mmWave session rerouted from the mmWave BS i is dropped upon returning from the sub-6 GHz BS N after exactly k reroutes is

$$\left[\frac{\alpha(1-\pi_{N,N})\pi_r(1-\pi_{N,i})}{\alpha+\mu_{NR}}\right]^k \frac{\alpha(1-\pi_{N,N})\pi_r\pi_{N,i}}{\alpha+\mu_{NR}}. \quad (44)$$

Summing up (43) and (44) over all $k \geq 0$, one can produce another expression for the ongoing mmWave session drop probability $\pi_{O,i}$ in the form

$$\pi_{O,i} = \frac{\frac{\alpha}{\alpha+\mu_{NR}}\left(\pi_{N,N}+(1-\pi_{N,N})\pi_r\pi_{N,i}\right)}{1-\frac{\alpha}{\alpha+\mu_{NR}}(1-\pi_{N,N})\pi_r(1-\pi_{N,i})}. \quad (45)$$

Therefore, the sought probability $\pi_{O,i|N}$ is given as

$$\pi_{O,i|N} = \frac{\pi_{N,N}}{\pi_{N,N}+(1-\pi_{N,N})\pi_r\pi_{N,i}}. \quad (46)$$

Averaging across all the mmWave BSs, we finally establish

$$\pi_{O|N} = \frac{\sum_{i=1}^{N-1}\lambda_i(1-\pi_{N,i})\pi_{O,i|N}}{\sum_{i=1}^{N-1}\lambda_i(1-\pi_{N,i})}. \quad (47)$$

E. Capturing Retrial User Behavior

In practical cases, there might be an "after-effect" associated with the session drops. Particularly, a user can consider re-initiating a session that may change the system's overall behavior. There are two approaches to incorporating this behavior: (i) the current queuing framework can be utilized to approximate the retrial behavior, and (ii) a new queuing framework may be developed to capture such user behavior. Note that only the queuing part needs to be modified, while the parametrization part remains as-is.

Should one need to capture the retrial user behavior, the developed queuing framework has to be modified. However, the analysis of multi-server retrial queues is more difficult than that for the case without retrials. Explicit expressions for the stationary probabilities of the basic M/M/c/c queue were obtained only for $c = 1$ and $c = 2$ [45]. For $c \geq 3$, establishing an analytical solution for the stationary probability distribution is challenging [46]. Hence, one may not expect a solution for a queuing system with random resource requirements to appear soon.

Another approach relies on approximating the flow of retrial sessions. However, one should remember that the orbit sessions on average require more PRBs for service than the initially arriving customers. This is because these sessions are exactly the ones likely to be dropped upon arrival. Denote by $B(\rho, N, \{p_r\})$ the session drop probability in a system with offered load ρ, N servers, and resource requirements distribution $\{p_r\}$. Then, one needs to solve

$$\rho_{retrial} = (\rho_{initial}+\rho_{retrial})B(\rho_{initial}+\rho_{retrial}, N, \{q_r\}), \quad (48)$$

where $\{q_r\}$ is defined as

$$\{q_r\} = \frac{\rho_{initial}}{\rho_{initial}+\rho_{retrial}}\{p_r\} + \frac{\rho_{retrial}}{\rho_{initial}+\rho_{retrial}}\{\widetilde{p}_r\}, \quad (49)$$

where $\{\widetilde{p}_r\}$ is the resource requirements distribution of the blocked sessions in the system with N servers and the offered load $(\rho_{initial}+\rho_{retrial})$. A solution can be obtained iteratively. We start with $\rho_{retrial}$ and $\{q_r\} = \{p_r\}$. Substituting these into the right-hand side of (48), we obtain a new value of $\rho_{retrial}$, which is then used to evaluate the new resource requirements distribution of the blocked sessions $\{\widetilde{p}_r\}$. The new values of $\rho_{retrial}$ and $\{\widetilde{p}_r\}$ are substituted into the right-hand side of (49) to produce the new aggregate distribution $\{q_r\}$, and then the algorithm proceeds to its next iteration. It stops when the difference between the new and old values of $\rho_{retrial}$ is below the accuracy threshold ϵ.

TABLE II
PARAMETERS FOR NUMERICAL ASSESSMENT

Parameter	Value
mmWave carrier frequency	28 GHz
mmWave bandwidth	400 MHz
sub-6 GHz carrier frequency	3.5 GHz
sub-6 GHz bandwidth	100 MHz
Height of mmWave BS	10 m
Height of sub-6 GHz BS	30 m
Height of blockers	1.7 m
Blocker intensity	0.5 units/m^2
Height of UEs	1.5 m
Blocker radius	0.4 m
Blocker speed	1 m/s
Mean blocker movement duration	5 m
SNR blockage threshold	-9.47 dB
mmWave transmit power	35 dBm
Path loss exponent	2.1
mmWave cell-edge outage probability	0.05
STD of shadow fading	8.2/4 dB
Thermal noise	-174 dBm/Hz
mmWave blockage attenuation	20 dB
sub-6 GHz BS antenna array	8×4 elements
sub-6 GHz UE antenna array	4×4 elements
mmWave BS antenna array	32×4 elements
mmWave UE antenna array	4×4 elements
Cable losses	2 dB
Interference margin	3 dB
Mean session service time	30 s
Number of mmWave BSs in sub-6 GHz BS coverage	9
Number of clusters	5
Default sub-6 GHz session data rate	1 Mbps
Default mmWave session data rate	5 Mbps

VI. SELECTED NUMERICAL RESULTS

In this section, we numerically elaborate on the joint performance of sub-6 GHz and mmWave deployments. We start with assessing our developed framework's accuracy and then proceed by studying the considered metrics, which include sub-6 GHz and mmWave system utilization, new and ongoing session drop probabilities for mmWave radio, and session drop probability for sub-6 GHz radio.

Throughout this section, we consider a two-cell scenario with a single mmWave BS located within the sub-6 GHz BS coverage. The mmWave BS is located at one-half of the coverage radius of the sub-6 GHz BS. Further, the arrival

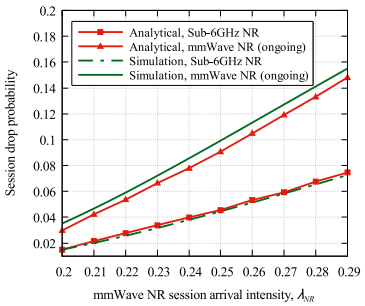

Fig. 3. Comparison of analytical and simulation results.

intensity at the mmWave BSs and the requested session data rate are λ_{NR} and c_{NR}, respectively, while the arrival intensity at the sub-6 GHz BS and the requested session data rate are λ_L and c_L, respectively. The default system parameters employed for our numerical assessment are collected in Table II.

A. Model Validation

Since the proposed analytical framework involves two radio access technologies with drastically different propagation features as well as traffic service processes with dynamic reroutes, we start by validating it against system-level simulations. To this aim, we implement a single-purpose simulation environment that follows the system model detailed in Section III. Our modeler is based on the discrete-event simulation (DES) concept. The statistics are collected during the steady-state period by using the method of batch means. The effect of residual correlations is removed by sampling the state of the system every 10 seconds of the simulation time. The beginning of a steady-state period is determined by using an exponentially weighted moving average test with a smoothening constant of 0.05.

The developed simulator accepts the input parameters specified in Table II but relaxes additional assumptions required for mathematical analysis. Particularly, (i) the propagation and blockage processes are modeled explicitly, and (ii) the resources requested from the sub-6 GHz and mmWave BSs are recalculated exactly based on the propagation conditions.

A comparison between the sub-6 GHz session drop probability and the ongoing mmWave session drop probability obtained using our mathematical framework and simulations is reported in Fig. 3 as a function of the mmWave session arrival rate, λ_{NR}, for the sub-6 GHz session data rate of $c_L = 1$ Mbps and the mmWave session data rate of $c_{NR} = 5$ Mbps. Here, we also consider the coinciding session durations of $\mu_L^{-1} = \mu_{NR}^{-1} = 30$ s, the intensity of sub-6 GHz session arrivals of $\lambda_L = 0.2$ sess./s, and the density of pedestrians of $\lambda_B = 0.1$ blockers/m^2. We also note that the confidence intervals remained within ± 0.01 of the absolute values, with the level of significance set to 0.95. Hence, we only demonstrate point estimates in Fig. 3.

As one may observe, the simulation results match the analytical findings tightly, with the maximum deviation of under 5%. Similar outcomes were observed for other input parameters and metrics of interest, including the system resource utilization and the new mmWave session drop probability.

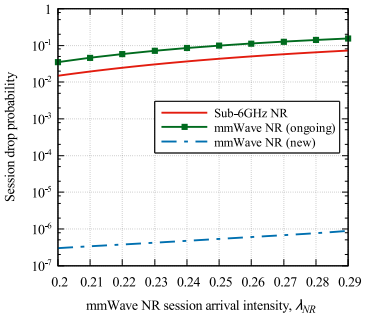

(a) As function of λ_{NR}, $\lambda_L = 0.2$ sess./s

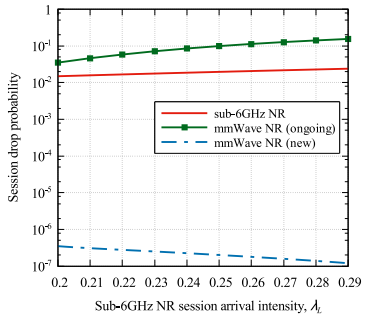

(b) As function of λ_L, $\lambda_{NR} = 0.2$ sess./s

Fig. 4. Session drop probabilities.

This implies that the core assumptions adopted for our mathematical framework do not substantially distort the studied parameters. In what follows, we thus rely on our analytical modeling to deliver the system performance assessment.

B. System Performance

We proceed by studying the system's response to the input parameters, which include the sub-6 GHz and mmWave session arrival intensities, session service time, requested session data rates, and density of blockers within the considered environment. Here, we focus on the system's operating regime by selecting the sub-6 GHz and mmWave session arrival rates such that the new sub-6 GHz session drop probability remains around 0.1.

We begin with the consideration of the session drop probability (see Fig. 4) as a function of the session arrival intensities, λ_L and λ_{NR}, for the sub-6 GHz session data rate of $c_L = 1$ Mbps, the mmWave session data rate of $c_{NR} = 5$ Mbps, the coinciding session durations of $\mu_L^{-1} = \mu_{NR}^{-1} = 30$ s, and the pedestrian density of $\lambda_B = 0.1$ blockers/m^2. As one may observe in Fig. 4(a), the new session drop probabilities increase for both mmWave and sub-6 GHz bands as mmWave session arrival intensity grows. For the practical values of mmWave and sub-6 GHz bandwidths, the new mmWave session drop probability remains extremely low, barely reaching 10^{-6} for $\lambda_{NR} \approx 0.3$ mmWave sess./s. However, once it is accepted, the chances of dropping the mmWave session become very high as the ongoing mmWave session drop probability gradually increases from 0.02 to around 0.1. These losses (caused by link blockages) eventually lead to reroutes to the sub-6 GHz BS. Hence, despite the high capacity of the 5G NR

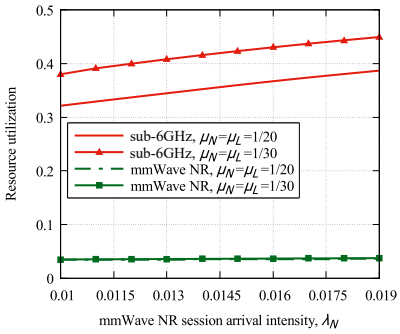

(a) As function of λ_{NR}, $\lambda_L = 0.2$ sess./s

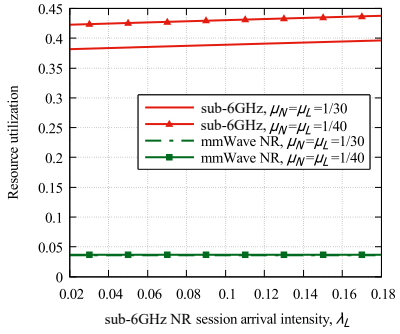

(b) As function of λ_L, $\lambda_{NR} = 0.2$ sess./s

Fig. 5. System resource utilization.

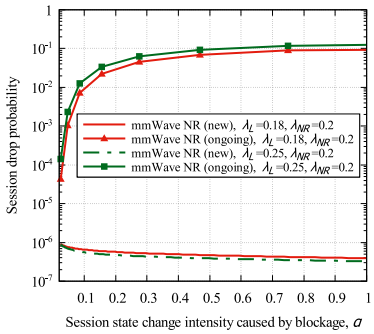

Fig. 6. Session drop probabilities as a function of λ_B.

infrastructure, the ultimate system performance may be subject to a significant degradation. Notably, the ongoing sub-6 GHz session drop probability is visibly lower than the new sub-6 GHz session drop probability. This is explained by the higher resource requirements of the mmWave sessions.

Considering the data reported in Fig. 4(b) for $\lambda_{NR} = 0.2$ sess./s, one may learn that increased arrival intensity of sub-6 GHz sessions leads to higher ongoing mmWave session drop probability. At the same time, the new mmWave session drop probability decreases. This can be explained by the fact that more sessions are being dropped during reroutes to the sub-6 GHz BS (due to a lack of available resources); hence, fewer sessions return to the mmWave BSs. However, this effect's magnitude is minor as the corresponding probability remains extremely low, between 10^{-7} and 10^{-6}. Further, as sub-6 GHz session intensity increases, the new mmWave session drop probability becomes lower. There are fewer sessions that return to the mmWave BSs due to higher ongoing mmWave session drop probabilities at sub-6 GHz BS, which reduces the mmWave BS resource utilization. It is also important to note that sub-6 GHz sessions experience much lower drop probability as compared to mmWave sessions at sub-6 GHz BS. As demonstrated further, this behavior is related to the capability of such systems to accept more sessions with lower resource requirements.

The system resource utilization for both bands is illustrated in Fig. 5. It is presented as a function of the session arrival rates, λ_L and λ_{NR}, for the sub-6 GHz session data rate of $c_L = 10$ Mbps, the mmWave session data rate of $c_{NR} = 20$ Mbps, the coinciding session durations of $\mu_L^{-1} = \mu_{NR}^{-1} = 30$ s, and the pedestrian density of $\lambda_B = 0.05$ blockers/m^2. With an increase in the arrival rate of the mmWave sessions, the radio resource utilization in both systems grows. Observe that an increase in the sub-6 GHz system resource utilization in Fig. 5(a) is caused solely by sessions rerouted from the mmWave BSs. It is important to note that the considered system operating conditions, where the sub-6 GHz session drop probability remains around 0.1, are associated with extremely low mmWave resource utilization of 0.1. Further, a growing mmWave session arrival rate does not affect the mmWave system resource utilization, which implies that the use of the sub-6 GHz radio does not allow for a noticeable improvement in the mmWave system performance.

Another valuable insight is that despite the high new sub-6 GHz session drop probability for the selected set of input parameters, the resource utilization of the sub-6 GHz radio is relatively low. This is because the mmWave sessions are temporarily rerouted to the sub-6 GHz BS. Recall that the service time of these sessions at the sub-6 GHz BS is determined by the outage duration with the mmWave BSs; hence, it is limited to only a few seconds. When accepted for service at the sub-6 GHz BS, these sessions utilize the sub-6 GHz resources for relatively short time intervals. Given that the resource requirements of these sessions are higher than those of the sub-6 GHz sessions, this also leads to increased sub-6 GHz session drop probability, wherein service duration is much longer. Therefore, the sub-6 GHz resources may be utilized inefficiently.

As was noted, the mean service duration for the mmWave sessions does not drastically affect the performance of the system at hand. One of the reasons behind it is that the numbers of reroutes to the sub-6 GHz band and their returns heavily depend on the interplay between the intensity of the UE state changes during the service time. We proceed by investigating this effect in Fig. 6, which displays the sub-6 GHz and the mmWave session drop probabilities as a function of the UE state change intensity α for the sub-6 GHz session data rate of $c_L = 1$ Mbps, the mmWave session data rate of $c_{NR} = 5$ Mbps, the coinciding session durations of $\mu_L^{-1} = \mu_{NR}^{-1} = 30$ s, and the intensities of sub-6 GHz and mmWave sessions of $\lambda_{NR} = \lambda_L = 0.2$ sess./s.

Analyzing the new and ongoing mmWave session drop probabilities, one may observe that higher blocker densities lead to more frequent drops of the ongoing sessions. For

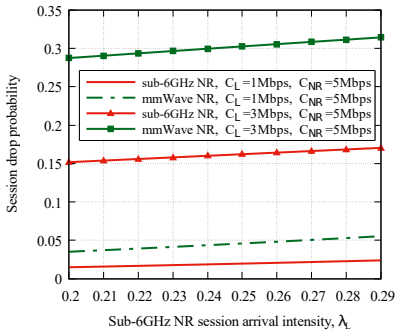

(a) Session drop probabilities, $\lambda_L = 0.2$ sess./s

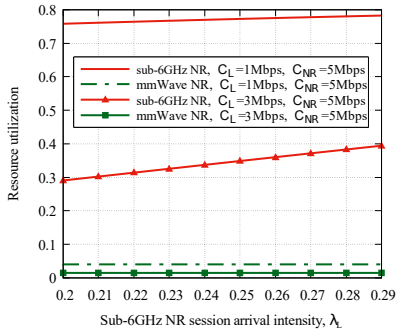

(b) System resource utilization, $\lambda_L = 0.2$ sess./s

Fig. 7. Session drop probabilities and resource utilization.

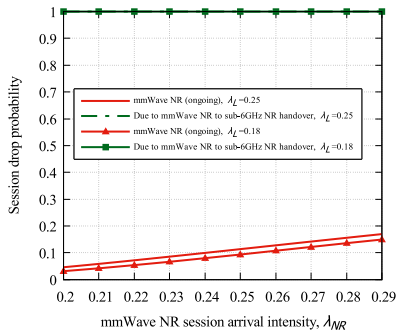

Fig. 8. Fraction of sessions dropped due to multi-band rerouting.

lower values of α, the probability of blockage during a session duration is negligible, and thus the ongoing mmWave session drop probability remains well below 10^{-2}. However, already for $\alpha = 0.2$ (6 blockages on average for the mean session duration of $\mu_{NR}^{-1} = 30$ s), the considered probability is 0.03, and it eventually reaches 0.1 for $\alpha = 1$. This effect is accompanied by a decrease in new mmWave session drop probability. However, it is not noticeable for the users as this probability is negligible, i.e., less than 10^{-6}.

We proceed by studying the response of our system to the sub-6 GHz request size distribution, c_L, which is illustrated in Fig. 7 as a function of the sub-6 GHz session arrival intensity for $\lambda_{NR} = 0.2$ sess./s, the coinciding session durations of $\mu_L^{-1} = \mu_{NR}^{-1} = 30$ s, and the pedestrian density of $\lambda_B = 0.1$ blockers/m^2. As one may see, the growing sub-6 GHz resource request values increase both the sub-6 GHz and the mmWave ongoing session drop probabilities. However, the impact on the former parameter is more significant. This behavior is a consequence of shorter service time durations for the mmWave sessions in the sub-6 GHz system, which yields the discussed resource capture effect. It is also interesting to note that the considered service processes at the sub-6 GHz and mmWave BSs are, in fact, tightly coupled and cannot be addressed in isolation. As evident from Fig. 7(b), changes in the sub-6 GHz traffic affect the resource utilization at the mmWave BSs via the ongoing mmWave session drop probability.

Finally, we quantify the impact of the reroutes (from sub-6 GHz to mmWave BSs and back) on the ongoing session drop probability. Particularly, the fraction of mmWave session drops as a result of the mmWave to sub-6 GHz reroutes, as well as the absolute values of the ongoing mmWave probabilities, are highlighted in Fig. 8 as a function of the sub-6 GHz session arrival intensity of $\lambda_L = 0.2$ sess./s, the coinciding sub-6 GHz and mmWave session service times of 30 s, the sub-6 GHz session data rate of $c_L = 1$ Mbps, the mmWave session data rate of $c_{NR} = 5$ Mbps, and the blocker density of $\lambda_B = 0.1$ blockers/m^2. Clearly, rerouting from mmWave to sub-6 GHz BS has a major impact on the ongoing session drop probability. It is responsible for the session drops since only a minor fraction of the mmWave sessions are dropped due to reroutes from sub-6 GHz to mmWave BSs.

VII. Conclusions

Multi-band radio connectivity allows for a joint use of microwave and mmWave system resources to improve service continuity for 5G NR sessions. Combining the tools of stochastic geometry and queuing theory, we constructed an integrated mathematical framework that captures the wireless operation of sub-6 GHz and mmWave technologies as well as the coupled service processes of sub-6 GHz and mmWave sessions. The framework quantifies the key user- and system-centric performance indicators, including the new sub-6 GHz session and the new/ongoing mmWave session drop probabilities, and the sub-6 GHz and mmWave radio resource utilization.

Numerically, we demonstrated that the service processes of sub-6 GHz and mmWave sessions are tightly interconnected and cannot be considered in isolation. Particularly, even minor changes in the sub-6 GHz traffic affect the serving of mmWave sessions. Crucially, the presence of mmWave traffic drastically impacts the sub-6 GHz radio performance. Depending on the implementation of multi-band connectivity, there may be a need to protect the sub-6 GHz traffic while aiming at improved session continuity. With respect to the mmWave sessions, poor performance was observed when the intensity of the UE state changes remained high, thus leading to frequent reroutes from mmWave to sub-6 GHz BSs and back during the service time of a session.

From the practical perspective, the effect of multi-band mmWave/sub-6 GHz connectivity is relatively mild. We envision that multi-band operation has to be complemented with other means to improve session continuity in 5G NR systems, such as mmWave multi-connectivity [11] and guard capacity

[19], [18]. Our proposed framework is a useful tool for the system designers to understand when further measures are needed depending on the intended system performance.

REFERENCES

[1] Fujitsu, "Fujitsu and Qualcomm complete 5G data calls in Sub-6 GHz and mmWave spectrum bands," Available at: https://www.fujitsu.com/global/about/resources/news/press-releases/2019/0822-01.html, Accessed 09.01.2021., Tech. Rep.

[2] Qualcomm, "The 5G rollout for developers: Roadmap for mobile innovation," Avialable at: https://www.qualcomm.com/news/onq/2019/09/03/5g-rollout-roadmap, Accessed 09.01.2021., Tech. Rep.

[3] ITU-R, "Minimum requirements related to technical performance for IMT-2020 radio interface," ITU-R M.2410, Nov. 2017.

[4] A. Ghosh, R. Ratasuk, and F. Vook, "NR radio interface for 5G verticals," *5G Verticals: Customizing Applications, Technologies and Deployment Techniques*, pp. 57–91, 2020.

[5] GSMA, "5G implementation guidelines," Available at https://www.gsma.com/futurenetworks/wp-content/uploads/2019/03/5G-Implementation-Guideline-v2.0-July-2019.pdf, Accessed 09.01.2021, Tech. Rep., 2019.

[6] G. R. MacCartney, S. Deng, S. Sun, and T. S. Rappaport, "Millimeter-wave human blockage at 73 GHz with a simple double knife-edge diffraction model and extension for directional antennas," in *VTC-Fall*. IEEE, 2016, pp. 1–6.

[7] M. Gapeyenko, A. Samuylov, M. Gerasimenko, D. Moltchanov, S. Singh, M. R. Akdeniz, E. Aryafar, N. Himayat, S. Andreev, and Y. Koucheryavy, "On the temporal effects of mobile blockers in urban millimeter-wave cellular scenarios," *IEEE Transactions on Vehicular Technology*, vol. 66, no. 11, pp. 10 124–10 138, 2017.

[8] 3GPP, "Study on channel model for frequencies from 0.5 to 100 GHz (Release 14)," 3GPP TR 38.901 V14.1.1, July 2017.

[9] N. Seitz, "ITU-T QoS standards for IP-based networks," *IEEE Communications Magazine*, vol. 41, no. 6, pp. 82–89, 2003.

[10] 3GPP, "NR; Multi-connectivity; stage 2 (Release 16)," 3GPP TS 37.340 V16.0.0, December 2019.

[11] R. Kovalchukov, D. Moltchanov, V. Begishev, S. Andreev, Y. Koucheryavy, and K. Samouylov, "Improved Session Continuity in 5G NR with Use of Multi-Connectivity and Guard Bandwidth," in *IEEE GLOBECOM*, 2018, pp. 1–7.

[12] M. Höyhtyä, O. Apilo, and M. Lasanen, "Review of latest advances in 3GPP standardization: D2D communication in 5G systems and its energy consumption models," *Future Internet*, vol. 10, no. 1, p. 3, 2018.

[13] G. Brown, "Exploring 5G New Radio: use cases. capabilities & timeline," *Qualcomm White Paper*, 2016.

[14] G. R. MacCartney, T. S. Rappaport, and S. Rangan, "Rapid fading due to human blockage in pedestrian crowds at 5G millimeter-wave frequencies," in *GLOBECOM 2017*. IEEE, 2017, pp. 1–7.

[15] T. Bai and R. W. Heath, "Coverage analysis for millimeter wave cellular networks with blockage effects," in *2013 IEEE Global Conference on Signal and Information Processing*. IEEE, 2013, pp. 727–730.

[16] M. Gapeyenko, A. Samuylov, M. Gerasimenko, D. Moltchanov, S. Singh, E. Aryafar, S.-p. Yeh, N. Himayat, S. Andreev, and Y. Koucheryavy, "Analysis of human-body blockage in urban millimeter-wave cellular communications," in *Communications (ICC), 2016 IEEE International Conference on*. IEEE, 2016, pp. 1–7.

[17] A. Samuylov, M. Gapeyenko, D. Moltchanov, M. Gerasimenko, S. Singh, N. Himayat, S. Andreev, and Y. Koucheryavy, "Characterizing spatial correlation of blockage statistics in urban mmwave systems," in *IEEE Globecom Workshops (GC Wkshps)*, December 2016, pp. 1–7.

[18] D. Moltchanov, A. Samuylov, M. Gapeyenko, N. Himayat, S. Andreev, and Y. Koucheryavy, "Improving session continuity with bandwidth reservation in mmwave communications," *IEEE Wir. Comm. Let.*, vol. 8, no. 1, pp. 105–108, 2018.

[19] V. Begishev, D. Moltchanov, E. Sopin, A. Samyilov, S. Andreev, Y. Koucheryavy, and K. Samuilov, "Quantifying the impact of guard capacity on session continuity in 3GPP New Radio systems," *IEEE Trans. on Veh. Tech.*, vol. 1, no. 1, pp. 1–15, 2019.

[20] V. Petrov, M. A. Lema, M. Gapeyenko, K. Antonakoglou, D. Moltchanov, F. Sardis, A. Samuylov, S. Andreev, Y. Koucheryavy, and M. Dohler, "Achieving end-to-end reliability of mission-critical traffic in softwarized 5G networks," *IEEE JSAC*, vol. 36, no. 3, pp. 485–501, 2018.

[21] M. S. Omar, M. A. Anjum, S. A. Hassan, H. Pervaiz, and Q. Niv, "Performance analysis of hybrid 5G cellular networks exploiting mmwave capabilities in suburban areas," in *ICC*. IEEE, 2016, pp. 1–6.

[22] V. F. Monteiro, D. A. Sousa, T. F. Maciel, F. R. P. Cavalcanti, C. F. e Silva, and E. B. Rodrigues, "Distributed RRM for 5G multi-RAT multiconnectivity networks," *IEEE Systems Journal*, vol. 13, no. 1, pp. 192–203, 2018.

[23] G. Ghatak, A. De Domenico, and M. Coupechoux, "Coverage analysis and load balancing in hetnets with millimeter wave multi-rat small cells," *IEEE Transactions on Wireless Communications*, vol. 17, no. 5, pp. 3154–3169, 2018.

[24] 3GPP, "Study on channel model for frequencies from 0.5 to 100 GHz (Release 14)," 3GPP TR 38.901 V14.1.1, July 2017.

[25] M. Gapeyenko, V. Petrov, D. Moltchanov, S. Andreev, Y. Koucheryavy, M. Valkama, M. R. Akdeniz, and N. Himayat, "An analytical representation of the 3GPP 3D channel model parameters for mmWave bands," in *Proceedings of the 2nd ACM Workshop on Millimeter Wave Networks and Sensing Systems*. ACM, 2018, pp. 33–38.

[26] P. Nain, D. Towsley, B. Liu, and Z. Liu, "Properties of random direction models," in *IEEE 24th Annual Joint Conference of the IEEE Computer and Communications Societies*, vol. 3, March 2005, pp. 1897–1907.

[27] ITU-R, "Propagation data and prediction methods required for the design of terrestrial line-of-sight systems," ITU-R P 530-17, Nov. 2017.

[28] V. Petrov, M. Komarov, D. Moltchanov, J. M. Jornet, and Y. Koucheryavy, "Interference and SINR in millimeter wave and terahertz communication systems with blocking and directional antennas," *IEEE Transactions on Wireless Communications*, vol. 16, no. 3, pp. 1791–1808, March 2017.

[29] A. B. Constantine *et al.*, "Antenna theory: analysis and design," *Microstrip Antennas, John Wiley & Sons*, 2005.

[30] M. Gerasimenko, D. Moltchanov, M. Gapeyenko, S. Andreev, and Y. Koucheryavy, "Capacity of multiconnectivity mmwave systems with dynamic blockage and directional antennas," *IEEE Trans. on Veh. Tech.*, vol. 68, no. 4, pp. 3534–3549, 2019.

[31] 3GPP, "NR; Physical channels and modulation (Release 15)," 3GPP TR 38.211, Dec 2017.

[32] S. Ross, *Introduction to probability models*. Academic Press, 2010.

[33] R. Kovalchukov, D. Moltchanov, A. Samuylov, A. Ometov, S. Andreev, Y. Koucheryavy, and K. Samouylov, "Evaluating SIR in 3D millimeter-wave deployments: Direct modeling and feasible approximations," *IEEE Transactions on Wireless Communications*, vol. 18, no. 2, pp. 879–896, 2019.

[34] M. Gapeyenko, V. Petrov, D. Moltchanov, S. Andreev, N. Himayat, and Y. Koucheryavy, "Flexible and reliable UAV-assisted backhaul operation in 5G mmwave cellular networks," *IEEE JSAC*, vol. 36, no. 11, pp. 2486–2496, 2018.

[35] D. J. Daley, "The busy period of the M/GI/∞ queue," *Queueing Systems*, vol. 38, no. 2, pp. 195–204, 2001.

[36] J. G. Kemeny, J. L. Snell *et al.*, *Finite markov chains*. van Nostrand Princeton, NJ, 1960, vol. 356.

[37] P. Kuehn, "Approximate analysis of general queuing networks by decomposition," *IEEE Transactions on Communications*, vol. 27, no. 1, pp. 113–126, 1979.

[38] E. Sopin, K. Ageev, and K. Samouylov, "Approximate analysis of the limited resources queuing system with signals," in *Proceedings of 33rd European Conference for Modeling and Simulation (ECMS)*. ECMS, 2019.

[39] O. Vikhrova, "About Probability Characteristics Evaluation in Queuing System with Limited Resources and Random Requirements," *Discrete and Continuous Models and Applied Computational Science*, vol. 25, no. 3, pp. 209–216, 2017.

[40] V. Naumov, K. Samuilov, and A. Samuilov, "On the Total Amount of Resources Occupied by Serviced Customers," *Automation and Remote Control*, vol. 77, no. 8, pp. 1419–1427, 2016.

[41] K. Samouylov, E. Sopin, and O. Vikhrova, "Analyzing blocking probability in LTE wireless network via queuing system with finite amount of resources," in *Dudin A., Nazarov A., Yakupov R. (eds) Information Technologies and Mathematical Modelling - Queueing Theory and Applications. ITMM 2015*. Springer, 2015.

[42] V. Naumov, K. Samoulov, N. Yarkina, E. Sopin, S. Andreev, and A. Samuylov, "LTE performance analysis using queuing systems with finite resources and random requirements," in *2015 7th International Congress on Ultra Modern Telecommunications and Control Systems and Workshops (ICUMT)*. IEEE, 2015, pp. 100–103.

[43] K. Samoulov, Y. Gaidamaka, and E. Sopin, "Simplified analysis of queueing systems with random requirements," in *Pilz J., Rasch D., Melas V., Moder K. (eds) Statistics and Simulation. IWS 2015. Springer Proceedings in Mathematics & Statistics*. Springer, 2018, pp. 381–390.

[44] E. Sopin, K. Ageev, E. Markova, O. Vikhrova, and Y. Gaidamaka, "Performance Analysis of M2M Traffic in LTE Network Using Queuing Systems with Random Resource Requirements," *Automatic Control and Computer Sciences*, vol. 52, no. 5, pp. 345–353, 2018.
[45] J. Cohen, "Basic problems of telephone traffic theory and the influence of repeated calls," *Pillips Telecomm. Rev.*, vol. 18, no. 2, 1957.
[46] C. Pearce, "Extended continued fractions, recurrence relations and two-dimensional Markov processes," *Advances in Applied Probability*, pp. 357–375, 1989.